



Pharmacophore-fusing design of pyrimidine sulfonylacetanilides as potent non-nucleoside inhibitors of HIV-1 reverse transcriptase

Yali Sang^{a,b}, Christophe Pannecouque^d, Erik De Clercq^d, Chunlin Zhuang^{a,b,*}, Fener Chen^{a,b,c,*}

^a Engineering Center of Catalysis and Synthesis for Chiral Molecules, Department of Chemistry, Fudan University, Shanghai 200433, People's Republic of China

^b Shanghai Engineering Center of Industrial Asymmetric Catalysis for Chiral Drugs, Shanghai 200433, People's Republic of China

^c Institute of Pharmaceutical Science and Technology, Zhejiang University of Technology, 18 Chao Wang Road, 310014 Hangzhou, People's Republic of China

^d Rega Institute for Medical Research, KU Leuven, Herestraat 49, B-3000 Leuven, Belgium

ARTICLE INFO

Keywords:

Biphenyl
Rilpivirine
Sulfonylacetanilide
DAPYs
HIV-1
Reverse transcriptase

ABSTRACT

Twenty-seven derivatives (40–66) were generated by pharmacophore fusing of sulfonylacetanilide-diarylpyrimidine (1) with rilpivirine or biphenyl-diarylpyrimidines. They displayed up to single-digit nanomolar activity against wild-type (WT) virus and various drug-resistant mutant strains in HIV-1-infected MT-4 cells, thereby targeting the reverse transcriptase (RT) enzyme. Compound 51 displayed exceptionally potent activity against WT virus ($EC_{50} = 6$ nM) and several mutant strains (L100I, $EC_{50} = 8$ nM, K103N, $EC_{50} = 6$ nM, Y181C, $EC_{50} = 26$ nM, Y188L, $EC_{50} = 122$ nM, E138K, $EC_{50} = 26$ nM). The structure-activity relationships of the newly obtained pyrimidine sulfonylacetanilides were also elucidated. Molecular docking analysis explained the activity and provided a structural insight for follow-up research.

1. Introduction

Acquired immune deficiency syndrome (AIDS) has continued to be a devastating global health problem. With the development of new potent antiviral drugs, the deaths (0.77 million) of AIDS have been globally controlled in 2018 [1] compared to 1.9 million in 2003 [2]. Etiologically, AIDS is primarily caused by human immunodeficiency virus (HIV) [3]. Reverse transcriptase (RT) plays a critical role in the HIV-1 infective life cycle, and it has been recognized as an important therapeutic target of HIV infection [4]. Efficient strategies were used to conduct the discovery of potent anti-HIV-1 small molecules by inhibition of this enzyme, such as conformation restriction strategy [5], molecular modelling [6,7] and virtual screening approaches [8]. Among these small-molecule RT inhibitors, more than 50 kinds of non-nucleoside reverse transcriptase inhibitors (NNRTIs) were identified [9–10]. They specially bind to the RT at an allosteric site, located about 10 Å away from the DNA polymerase catalytic site [11]. During the process of ligand binding, conformational changes occur in the orientation of some functional residues (e.g. Tyr181 and Tyr188), leading to the development of the NNRTI binding pocket, namely NNIBP, accommodating the compounds [12]. These NNRTIs employ a similar binding conformation in the NNIBP, described as a “butterfly”, “horseshoe”, or “U” mode, providing valuable structural information for the design of new NNRTIs [13,14].

After the description of the first NNRTIs in the 1989–1990 [15,16], six NNRTI-type drugs, nevirapine (NVP), delavirdine (DLV), efavirenz (EFV), etravirine (ETR), rilpivirine (RPV) and doravirine (DOR), have been marketed [17]. The second generation NNRTIs, ETR and RPV, bearing the diarylpyrimidine (DAPY) scaffold, form a flexible “U” conformation with the RT enzyme, minimizing the loss of binding stability [18]. Accordingly, they possess a higher genetic barrier than the first generation NNRTIs (NVP, DLV, EFV), exhibiting excellent pharmacological effects against mutant viral strains [19]. Unfortunately, they were confronted by high cytotoxicity ($CC_{50} < 5$ μM) [20], and meanwhile, their effects are reduced by the emergence of new drug-resistant mutants upon long-term application, such as K103N and E138K [21]. Therefore, the development of new DAPY-type derivatives with favorable physicochemical profiles and better activity, especially toward mutant strains, is remains highly desirable.

2. Results and discussion

2.1. Design rationale

On the basis of the previous structure-activity relationships (SAR) of DAPY analogues [19,20–22], a pharmacophore model could be delineated for further optimizations (Fig. 1). In addition to the core

* Corresponding authors at: Engineering Center of Catalysis and Synthesis for Chiral Molecules, Department of Chemistry, Fudan University, Shanghai 200433, People's Republic of China.

E-mail addresses: zcnathan@163.com (C. Zhuang), rfchen@fudan.edu.cn (F. Chen).

<https://doi.org/10.1016/j.bioorg.2020.103595>

Received 1 December 2019; Received in revised form 14 January 2020; Accepted 18 January 2020

Available online 22 January 2020

0045-2068/ © 2020 Elsevier Inc. All rights reserved.

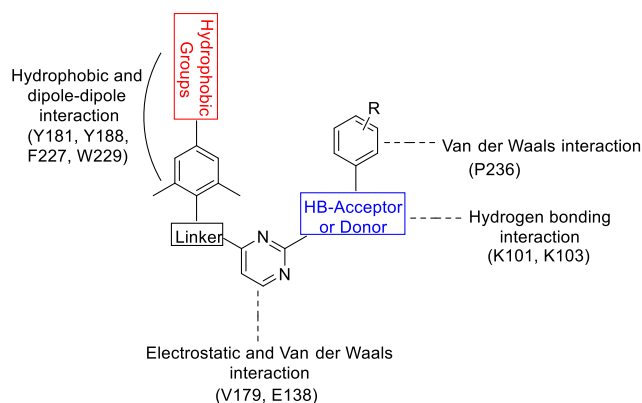


Fig. 1. A pharmacophore model of DAPYs.

diarylpyrimidine scaffold providing van der Waals and hydrophobic interactions, two features are critical to the antiviral activity. First, a vinyl or phenyl group is a suitable attachment on the left wing forming π - π interactions with Y181, Y188 and W229. Second, a hydrogen-bond (HB) acceptor or donor is favorable to produce hydrogen-bonding interactions with K101 and K103 as well as to modulate the physico-chemical properties of compounds.

Therefore, applying a pharmacophore fusing approach providing two privileged scaffolds to these two sites may reveal new chemical entities (NCE) and expand chemical space with more pharmacological effects [23]. The sulfonylacetanilide, making the compounds less toxic with favorable pharmacokinetic profiles, has been widely utilized, i.e., in matrix metalloproteinase inhibitors [24], gram-negative antibacterial agents [25], noncompetitive CXCL8 inhibitors [26]. Additionally, this motif has also been applied in potent HIV-1 inhibitors [27,28]. The etravirine-VRX-480773 hybrid (1) with the sulfonylacetanilide group previously discovered by our group showed great anti-HIV-1 activity [29]. This sulfonylacetanilide group was predicted to form two hydrogen bonds with the main chain of residues K101 and K103 [30–31], indicating its adaptation at the HB site of the model. The 4-cyanovinyl moiety of RPV (2) and a biphenyl group in our recent

disclosed compound (3) favorably influenced the antiviral activity against the drug-resistant strains [32]. The moiety can form π - π stacking interactions with Y181, Y188, F227, and W229, making the left ring region significantly adapt to the allosteric RT binding site. Thus, this fragment might be favorable at the hydrophobic site of the model. Collectively, the novel DAPY derivatives were designed by a pharmacophore fusing strategy on the basis of the present model (Fig. 2) in order to incorporate advantages to enhance antiviral potency against WT and drug-resistant HIV-1 viruses.

2.2. Chemistry

The synthetic route of the desired compounds 40–56 is outlined in Scheme 1. The key intermediates 9a–r were prepared from 4a–b by protection with a triphenylmethyl group, condensation with amines and deprotection. Compounds 11a–b were obtained via treating commercially available 10 with the intermediates 4'-hydroxy-[1,1'-biphenyl]-4-carbonitrile or (2E)-3-(4-hydroxy-3,5-dimethylphenyl)-2-propenenitrile, which was prepared following our established procedure [22,33]. Then, compounds 12a–b were easily prepared by oxidation [34], and they were reacted with 9a–r via the substitution reaction, leading to the formation of 13–39. Finally, 13–39 were reacted with 3-chloroperoxybenzoic acid to obtain pyrimidine sulfonylacetanilide derivatives 40–56. The desired compounds were determined by NMR and MS characterization.

2.3. Antiviral activity and binding prediction analysis

First, the acrylonitrile group of RPV was introduced to pyrimidine sulfonylacetanilides (1). Eight new compounds (40–47) were synthesized. They displayed promising anti-WT HIV-1 activity in the nanomolar range (Table 1). Compounds 40–41 showed EC_{50} values of 5–7 nM, which were similar to those of 1 (EC_{50} = 2 nM), ETR (EC_{50} = 6 nM) and RPV (EC_{50} = 1 nM). The results showed the acrylonitrile moiety was a suitable attachment for improving anti-HIV-1 potency. Then, the anilide was extended by inserting one or two methylenes to explore the chemical space in the P236 loop (Fig. 1).

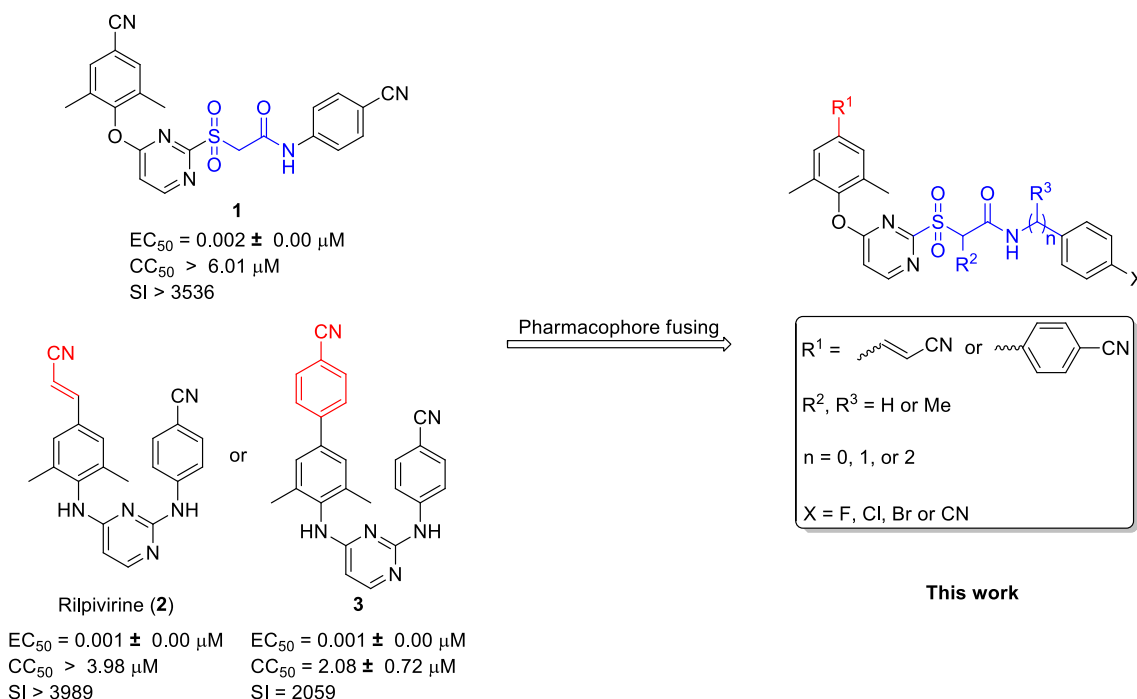
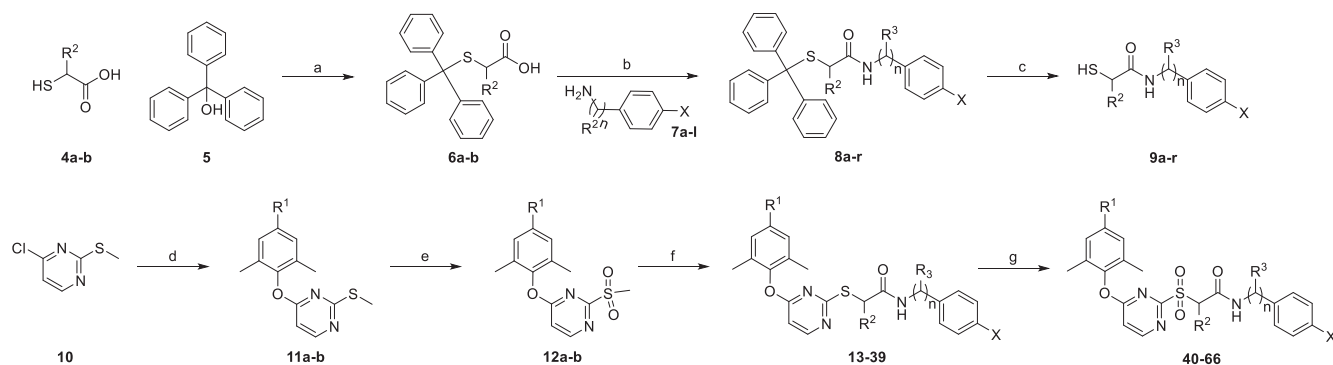


Fig. 2. Design of new pyrimidine sulfonylacetanilides by a pharmacophore fusing strategy.



Scheme 1. Synthesis of compounds 40–66^a. Reagents and conditions: (a) TFA, CHCl₃, 30 °C, 3 h; (b) DIPEA, PyBOP, DCM, 25 °C, 15 h; (c) (Et)₃SiH, TFA, DCM, 0–25 °C, 3 h; (d) 4'-hydroxy-[1,1'-biphenyl]-4-carbonitrile or (2E)-3-(4-hydroxy-3,5-dimethylphenyl)-2-propenenitrile, K₂CO₃, DMF, 80 °C, 4–6 h; (e) *m*-CPBA, DCM, 0–25 °C, 10 h; (f) **9a-r** Na₂CO₃, acetone, H₂O, 0–25 °C, 5 h; (g) *m*-CPBA, DCM, –45–25 °C, 12 h.

However, the structure-activity relationship (SAR) analysis highlighted the importance of aniline with dramatically decreased activity of compounds **42–47**. Compounds containing one methylene (**42–44**) had EC₅₀ values of 0.944–1.854 μM. Those containing two methylene (**45–47**) showed EC₅₀ values of 0.163–0.794 μM. The cytotoxicity was decreased to be lower than the reference compounds.

Then, the binding modes of **40** (EC₅₀ = 5 nM) and **42** with one more methylene (EC₅₀ = 1.854 μM) bound to wild-type RT were predicted. They exhibited several common features (Fig. 3). (1) These compounds employed a similar “U” mode binding conformation in the NNIBP. (2) Both of their left wing structures formed π-π stacking interactions with the residues Y181, Y188, F227, and W229. The cyano group additionally formed hydrogen interactions with Y188 (CN⋯H–O, distance = 3.2 Å for **40**, 2.1 Å for **42**) and residue K223 (CN⋯H–N, distance = 2.7 and 3.1 Å for **40**, 3.4 Å for **42**). Differently, the performance of sulfonylacetamide fragment in the NNIBP offered an explanation for their distinct activity. The sulfonylacetamide carbonyl group of **40** had a hydrogen-bonding interaction with K103 (C=O⋯H–N, distance: 2.0 Å). And the anilineformed two hydrogen bonds with the hydroxyl group of Y318 (N–H⋯O–H, distance: 3.4 Å) and residue P236 (N–H⋯O=C, distance = 3.0 Å) (Fig. 3A). For compound

42, although the hydrogen bond between the sulfonyl oxygen and K103 (O=S=O⋯H–N, distance: 2.5 Å) was observed, the extended right wing missed these essential features especially the benzylamine locating outside P236 loop (Fig. 3B).

Next, the biphenyl moiety was introduced to obtain biphenyl-pyrimidine sulfonylacetanilides (**48–51**). They exhibited great activity with EC₅₀ values of 6–34 nM against WT HIV-1 (Table 2). Compound **50** with a bromo group and **51** with a cyano group had similar single-digit nanomolar activity and SI values of ~4000. Similar extension on the P236 loop was performed with one more methylene (**52–55**), leading to reduced activity (EC₅₀ = 1.28–> 6.41 μM). Compound **55** with a cyano group had the highest activity (EC₅₀ = 1.28 μM) in these four new DAPYs. Extending with two more methylenes (compounds **56–58**) was still unfavorable to the activity. If a methyl group was introduced at the sulfone side into **49** and **51**, the corresponding compounds **59–60** had similar antiviral activity at low nanomolar range, and low cytotoxicity was observed, indicating the tolerance of methyl moiety on sulfonamide fragment. However, the methyl group did not increase the activity of compounds **61–63** or **64–66** compared with compounds **52–54**.

Then, the compounds exhibiting anti-WT HIV-1 activity in the nanomolar range were selected to be further evaluated against single-(L100I, K103N, Y181C, Y188L and E138K) and double-mutant viral strains (F227L + V106A and RES056) in MT-4 cells, as well as for their inhibitory ability against HIV-1 RT enzyme (Table 3). As expected, these compounds exhibited increased inhibitory activities against single-mutant virus strains with the exception of Y188L, while retaining inhibitory activity against the HIV-1 RT enzyme. Compound **40** exhibited great inhibitory activity against K103N with an EC₅₀ of 0.006 μM, which was superior to the references NVP, EFV (EC₅₀ = 0.102, > 10.075 μM, respectively). Compound **41** was active against L100I, K103N, Y181C, and E138K (EC₅₀ = 0.009, 0.007, 0.021 and 0.015 μM, respectively), comparable to that of ETR (EC₅₀ = 0.007, 0.003, 0.012 and 0.007 μM, respectively). Compound **51** showed low nanomolar EC₅₀ values toward all of the mutant strains. Notably, it had an EC₅₀ of 0.008 μM toward the L100I and 0.026 μM toward E138K, which was more potent than the parent compound **1** (EC₅₀ = 0.067 μM and 0.310 μM, respectively). Meanwhile, **51** was the most potent inhibitor toward the Y188L mutant (EC₅₀ = 0.122 μM) and dual mutant variants RES056 (EC₅₀ = 0.642 μM) and F227L + V106A (EC₅₀ = 0.226 μM). This was comparable to EFV and better than NVP.

Docking analysis indicated that the best compound **51** formed strong interactions with a number of key residues in the NNIBP (Fig. 4). First, the biphenyl fragment fitted well into the hydrophobic site (Y181, Y188, F227, and W229) and the hydrogen bonds between **51** and residues Y188 and K223 were retained, consistent with that of **40**. Second, the sulfonylacetamide moiety protruded into the Pro236 loop. A hydrogen-bonding interaction (N–H⋯O=C, distance = 2.2 Å) between the amino hydrogen of the sulfonylacetamide fragment and the

Table 1
Activity and cytotoxicity of compounds 40–47 against WT HIV-1 strain in MT-4

Compounds	n	X	HIV-1 (WT)	CC ₅₀ (μM) ^b	SI ^c
			EC ₅₀ (μM) ^a		
40	0	F	0.005 ± 0.00	19.5 ± 6.43	3900
41	0	Cl	0.007 ± 0.00	4.29 ± 0.97	613
42	1	F	1.854 ± 0.08	5.29 ± 0.35	3
43	1	Cl	> 1.43	1.43 ± 0.54	< 1
44	1	Br	0.944 ± 0.27	3.37 ± 1.25	4
45	2	F	0.163 ± 0.02	55.53 ± 47.19	340
46	2	Cl	0.490 ± 0.11	24.46 ± 9.97	50
47	2	Br	0.794 ± 0.24	39.23 ± 8.55	49
1			0.002 ± 0.00	> 6.01	> 3005
ETR			0.006 ± 0.00	> 4.61	> 768
RPV [16]			0.001 ± 0.00	> 3.98	3980

^a EC₅₀: The effective concentration required to protect MT-4 cells against viral cytopathicity by 50%.

^b CC₅₀: The cytotoxic concentration of the compound that reduced the normal uninfected MT-4 cell viability by 50%.

^c SI: selectivity index, ratio CC₅₀/EC₅₀ (WT).

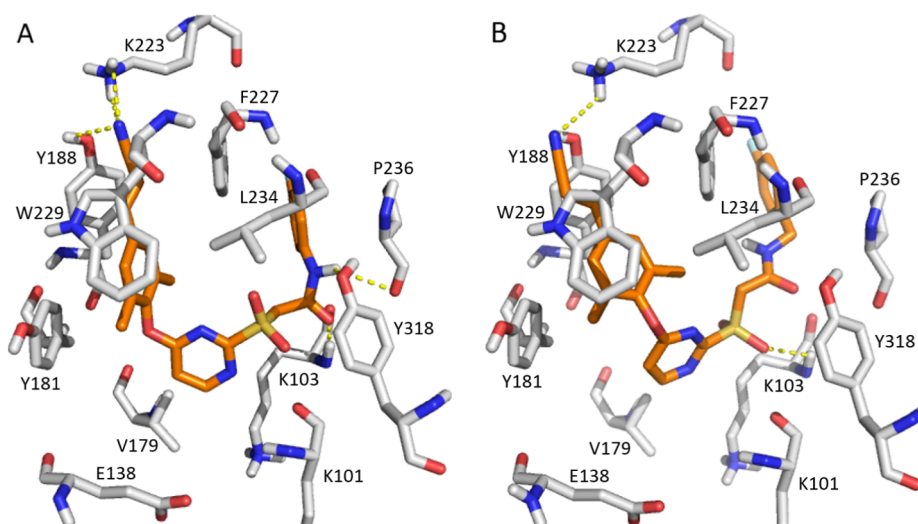


Fig. 3. Predicted binding modes of **40** (A), and **42** (B) with the WT HIV-1 RT crystal structure (PDB: 6CON). Hydrogen bonds are indicated as yellow dashed lines. The Figure was generated using PyMol (<http://pymol.sourceforge.net/>).

Table 2

Activity and cytotoxicity of compounds 48–66 against HIV-1 (WT) strain in MT-

Compounds	n	R ²	R ³	X	HIV-1 (WT)	CC ₅₀ (μM) ^b	SI ^c
					EC ₅₀ (μM) ^a		
48	0	H	–	F	0.023 ± 0.01	9.15 ± 3.95	398
49	0	H	–	Cl	0.034 ± 0.01	7.41 ± 3.18	218
50	0	H	–	Br	0.007 ± 0.00	26.91 ± 1.79	3844
51	0	H	–	CN	0.006 ± 0.00	24.44 ± 1.63	4073
52	1	H	H	F	> 6.41	6.41 ± 0.96	< 1
53	1	H	H	Cl	> 3.86	3.86 ± 0.98	< 1
54	1	H	H	Br	> 3.57	3.57 ± 0.91	< 1
55	1	H	H	CN	1.28 ± 0.69	51.23 ± 13.48	40
56	2	H	H	F	3.62 ± 1.86	15 ± 8.78	4
57	2	H	H	Cl	> 8.27	8.26 ± 1.94	< 1
58	2	H	H	Br	> 8.44	8.44 ± 0.94	< 1
59	0	Me	H	Cl	0.025 ± 0.01	16.35 ± 5.09	654
60	0	Me	H	CN	0.009 ± 0.00	15.38 ± 7.45	1708
61	1	Me	H	F	5.83 ± 2.11	20.19 ± 2.40	3
62	1	Me	H	Cl	> 12.18	12.17 ± 5.17	< 1
63	1	Me	H	Br	> 4.77	4.76 ± 0.89	< 1
64	1	H	Me	F	> 4.56	4.55 ± 0.75	< 1
65	1	H	Me	Cl	> 3.82	3.82 ± 1.12	< 1
66	1	H	Me	Br	> 3.21	3.21 ± 0.92	< 1
1					0.002 ± 0.00	> 6.01	> 3005
ETR					0.006 ± 0.00	> 4.61	> 768
RPV					0.001 ± 0.00	> 3.98	3980

^a EC₅₀: The effective concentration required to protect MT-4 cells against viral cytopathicity by 50%.

^b CC₅₀: The cytotoxic concentration of the compound that reduced the normal uninfected MT-4 cell viability by 50%.

^c SI: selectivity index, ratio CC₅₀/EC₅₀ (WT).

carbonyl group of K103 was formed (Fig. 4A). These interactions together may contribute to the potent antiviral activity. As shown in Fig. 4B-F, **51** was oriented into the pockets of the L100I, K103N, Y181C, Y188L, and E138K mutants and several common features (“U” binding

conformation, hydrogen bonds, hydrophobic and electrostatic interactions) were observed as in the wild-type RT. Especially, the N103 residue involved in additional hydrogen-bonding interactions with the pyrimidine nitrogen (N–H...N, distance = 2.7 Å) and aniline group (C=O...H–N, distance = 2.1 Å). In the Y181C and Y188L mutant, the π - π interactions were reduced compared with the wild-type RT, which together with the loss of the hydrogen bond between the cyano group and Y188L contributed to the loss of their antiviral activity. For E138K RT, an additional hydrogen bond between the pyrimidine core and K101 was observed (distance = 3.2 Å) for maintaining good activity.

3. Conclusion

In this study, two series of novel cyanovinyl- and biphenyl-pyrimidine sulfonylacetanilides were designed and synthesized via a pharmacophore fusing strategy. The most potent compound **51** displayed an EC₅₀ of 0.006 μM against HIV-1 wt strain, and EC₅₀ of 0.008, 0.006 μM, 0.026 μM, 0.122 μM, 0.026 μM against L100I, K103N, Y181C, Y188L, and E138K mutants. Molecular modelling further explained their activity and provided an example for pharmacophore fusing as a strategy in designing new HIV inhibitors.

A preliminary SAR was concluded (Fig. 5). (1) The cyanovinyl and biphenyl groups on the left wing were beneficial to enhance the antiviral ability. (2) Compound **59** and **60** with potent inhibitory activity against the HIV-1-infected cells showed the tolerance of methyl group on the sulfonylacetanilide fragment. (3) Modifications of the sulfonylacetamide group showed that extending the right wing was extremely detrimental to the antiviral ability.

4. Experimental

4.1. General

All reagents and solvents were purchased from commercial sources and used as received unless specified. Column chromatography was performed on silica gel (300–400 mesh). Thin-layer chromatography (TLC) was carried out on 0.25 mm silica gel plates and visualized with UV light ($\lambda = 254$ nm) and/or by staining with ethanolic phosphomolybdic acid (PMA) or iodine. Proton nuclear magnetic resonance (¹H NMR) and carbon nuclear magnetic resonance (¹³C NMR) spectra were recorded in DMSO-*d*₆ on a Bruker AV-400 spectrometer with tetramethylsilane (TMS) as the internal standard. Chemical shifts (δ) are given in ppm relative to TMS, coupling constants (*J*) in Hz. Melting

Table 3
Inhibitory activity of the selected compounds toward a panel of clinically relevant HIV-1 mutant strains and HIV-1 RT enzyme.

Compounds	EC ₅₀ (μM) ^a							IC ₅₀ (μM) ^b
	L100I	K103N	Y181C	Y188L	E138K	F227L + V106A	RES056	
40	0.033 ± 0.02	0.006 ± 0.00	0.045 ± 0.01	2.281 ± 1.07	0.023 ± 0.01	2.198 ± 0.47	0.440 ± 0.17	0.197 ± 0.03
41	0.009 ± 0.00	0.007 ± 0.00	0.021 ± 0.01	0.494 ± 0.10	0.015 ± 0.01	0.76 ± 0.16	0.228 ± 0.04	0.186 ± 0.01
48	0.177 ± 0.06	0.035 ± 0.01	0.528 ± 0.15	1.981 ± 1.00	0.112 ± 0.01	4.102 ± 2.33	3.536 ± 1.00	0.162 ± 0.12
49	0.116 ± 0.04	0.056 ± 0.01	0.275 ± 0.06	0.938 ± 0.17	0.197 ± 0.04	4.333 ± 0.53	4.209 ± 0.80	0.078 ± 0.01
50	0.049 ± 0.01	0.030 ± 0.00	0.114 ± 0.03	0.977 ± 0.14	0.091 ± 0.01	4.301 ± 1.60	4.999 ± 0.68	1.666 ± 1.47
51	0.008 ± 0.00	0.006 ± 0.00	0.026 ± 0.00	0.122 ± 0.04	0.026 ± 0.01	0.642 ± 0.09	0.226 ± 0.02	0.142 ± 0.01
59	0.069 ± 0.02	0.035 ± 0.01	0.146 ± 0.03	1.002 ± 0.09	0.114 ± 0.00	2.490 ± 0.42	3.294 ± 0.04	1.886 ± 0.33
60	0.106 ± 0.00	0.019 ± 0.04	0.242 ± 0.02	0.726 ± 0.01	0.041 ± 0.01	1.303 ± 0.13	1.433 ± 0.32	2.606 ± 0.74
1	0.067 ± 0.00	0.003 ± 0.00	0.017 ± 0.00	0.031 ^c	0.310 ± 0.07	0.127 ± 0.01	0.425 ± 0.31	0.065 ± 0.00
NVP	2.102 ± 0.75	> 10.075	> 15.867	> 15.867	0.210 ± 0.03	> 15.867	> 15.867	0.404 ± 0.09
EFV	0.044 ± 0.01	0.102 ± 0.05	0.007 ± 0.00	0.292 ± 0.04	0.006 ± 0.00	0.279 ± 0.10	0.273 ± 0.03	0.013 ± 0.01
ETR	0.007 ± 0.00	0.003 ± 0.00	0.012 ± 0.01	0.020 ± 0.01	0.007 ± 0.01	0.020 ± 0.01	0.045 ± 0.02	0.011 ± 0.01

^a EC₅₀: The effective concentration required to protect MT-4 cells against viral cytopathicity by 50%.

^b IC₅₀: inhibitory concentration of the test compound required to inhibit WT HIV-1 RT polymerase activity by 50%.

^c 0.031: the average of two EC₅₀ measurements.

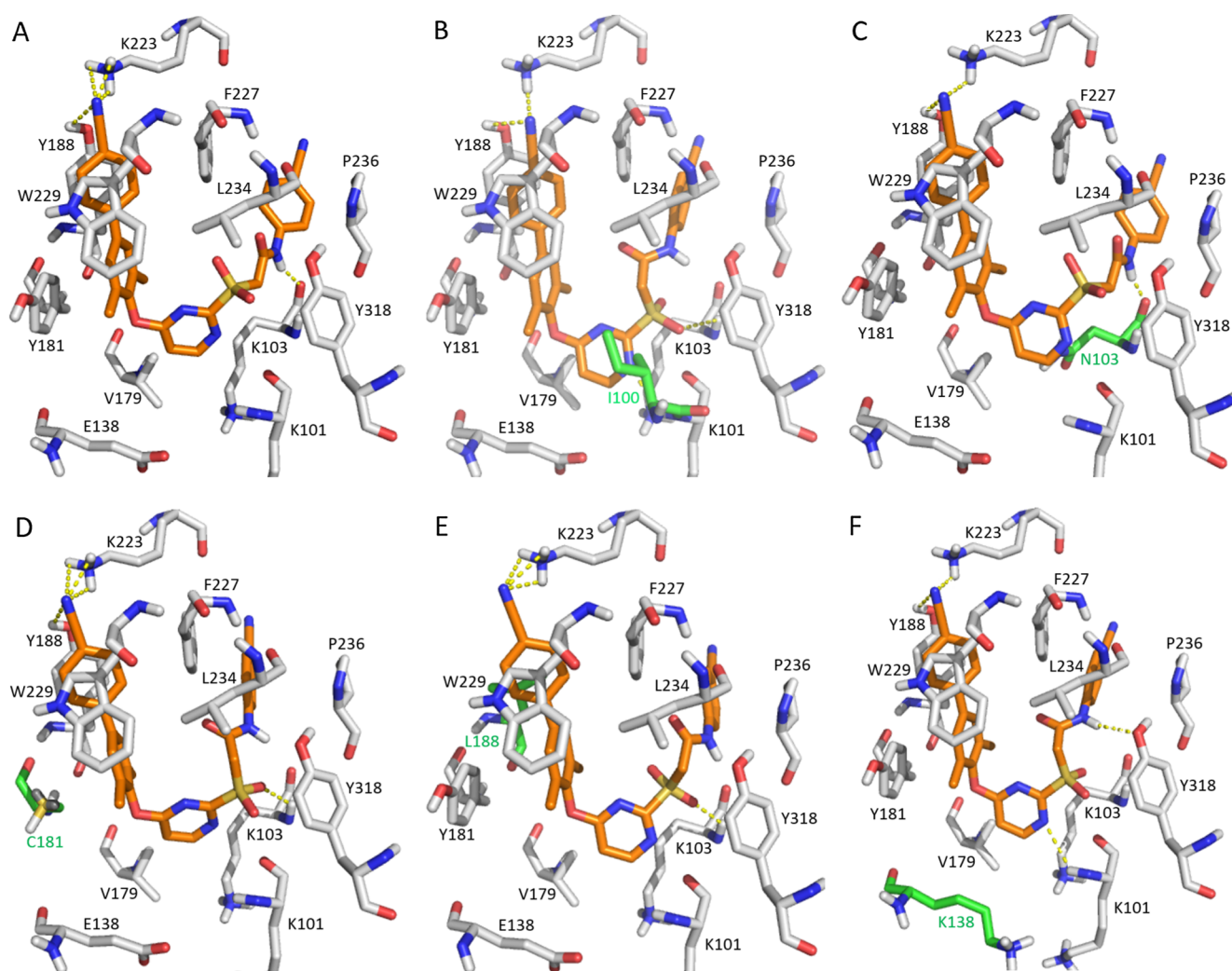


Fig. 4. Predicted binding modes of 51 with the HIV-1 wt (A), L100I (B), K103N (C), Y188C (D), Y188L (E) and E138K (F) mutant RT crystal structure (PDB: 6CON). Mutated residues are depicted as green sticks. Hydrogen bonds are indicated as yellow dashed lines. The Figure was generated using PyMol (<http://pymol.sourceforge.net/>).

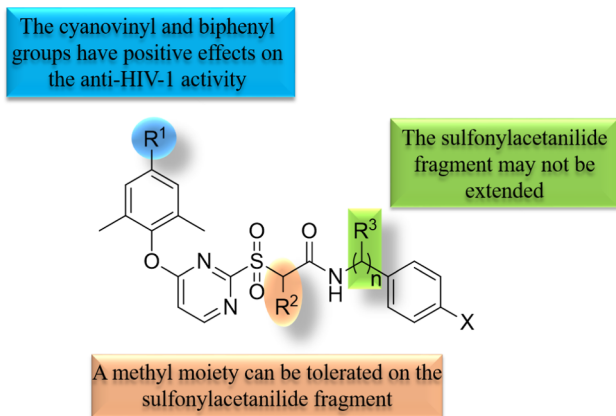


Fig. 5. A systematic summary of SAR.

points were measured on WRS-1B digital melting-point apparatus. EI-MS were recorded on an Agilent 6890N/5975 spectrometer and ESI-MS was recorded on a Waters Micromass Quattro Micro spectrometer. High-resolution mass spectra were recorded on a Bruker ApeXIII 7.0 TESLA FTMS.

4.2. General procedure for the preparation of compounds 6a-b

Triphenylmethanol (38.4 mmol, 1.0 eq) and TFA (49.9 mmol, 1.3 eq) was added to **4a-b** (38.4 mmol, 1.0 eq) in CHCl_3 (40 mL). The reaction mixture was stirred at 30 °C for 3 h. The volatiles were removed in vacuum. Crystallization with hexane yielded **6a-b** as white solid.

4.3. General procedure for the preparation of compounds 8a-r

DIPEA (7.2 mmol, 2.5 eq), PyBOP (3.6 mmol, 1.25 eq) and **6a-b** (2.9 mmol, 1.0 eq) in CH_2Cl_2 (20 mL) was stirred at 25 °C for 2 h, then, **7a-l** (3.2 mmol, 1.1 eq) was added. The mixture was stirred for another 13 h and quenched with H_2O (100 mL). The aqueous layer was extracted with CH_2Cl_2 (30 mL X 3) and the combined organic layers were washed with brine, and dried over anhydrous Na_2SO_4 . Purification of the crude reaction mixture was progressed by column chromatography (5–30% EtOAc/PE).

4.4. General procedure for the preparation of compounds 9a-r

TFA (19.0 mmol, 10.0 eq) and $(\text{Et})_3\text{SiH}$ (3.8 mmol, 2.0 eq) were added to **8a-r** (1.9 mmol, 1.0 eq) in CH_2Cl_2 (15 mL) at 0 °C. The mixture was stirred at 25 °C for 3 h. Volatiles were removed in vacuo. The crude product was crystallized from cold hexane to obtain the desired compounds as white solid.

4.5. General procedure for the preparation of compounds 11a-b

4'-hydroxy-[1,1'-biphenyl]-4-carbonitrile or (2E)-3-(4-hydroxy-3,5-dimethylphenyl)-2-propenenitrile (50 mmol, 1.0 equiv.) was dissolved in DMF (80 mL) in the presence of K_2CO_3 (150 mmol, 3.0 equiv.), followed by addition of the 4-chloro-2-(methylthio)pyrimidine (50 mmol, 1.0 equiv.). The reaction mixture was stirred at 80 °C for 4–6 h (monitored by TLC), and then the reaction was cooled to ambient temperature and poured into 400 mL H_2O yielding a precipitate. The precipitate was collected by filtration and the residue was then purified via column chromatography on silica gel, and eluted with EtOAc/PE to obtain **11a-b** as white solid.

4.6. General procedure for the preparation of compounds 12a-b

m-CPBA (150 mmol, 3.0 equiv.) was added to a solution of **11a-b** (50 mmol, 1.0 equiv.) in CH_2Cl_2 (150 mL) in small portions at 0 °C. Stirring was continued for an additional 10 h at 25 °C until complete consumption of starting material as judged by TLC. The reaction mixture was washed by sat. Na_2SO_3 , sat. Na_2CO_3 , water and brine. The organic layer was dried over anhydrous Na_2SO_4 , filtered and condensed under reduced pressure. The residue was then purified via column chromatography on silica gel, and eluted with EtOAc/PE to obtain **12a-b** as white solid.

4.7. General procedure for the preparation of compounds 13–39

A solution of intermediate **9a-r** (1 mmol, 1 equiv.) in acetone (3 mL) was added dropwise to an ice-cold mixture of **12a-b** (1 mmol, 1.0 equiv.) and Na_2CO_3 (2.5 mmol, 2.5 equiv.) in acetone/ H_2O (5/2 mL) over 20 min. The reaction mixture was stirred overnight at 25 °C, after which TLC analysis indicated the reaction was complete. The reaction mixture was neutralized with concentrated hydrochloric acid, filtered off, washed with cold water and dried to afford the desired product.

4.8. General procedure for the preparation of compounds 40–66

m-CPBA (1.25 mmol, 2.5 equiv.) was added to a solution of **13–39** (0.5 mmol, 1.0 equiv.) in CH_2Cl_2 (5 mL) in small portions at –45 °C. When the temperature gradually increased, stirring was continued until complete consumption of starting material as judged by TLC. The reaction mixture was washed by sat. Na_2SO_3 , sat. Na_2CO_3 , water and brine. The organic layer was dried over anhydrous Na_2SO_4 , filtered and condensed under reduced pressure. The crude product was purified by column chromatography on silica gel (EtOAc/PE = 1:5) to provide target compounds **40–66**.

4.8.1. (E)-2-((4-(4-(2-cyanovinyl)-2,6-dimethylphenoxy)pyrimidin-2-yl)sulfonyl)-N-(4-fluorophenyl)acetamide (40)

Yield: 80%. mp: 140.1–142.7 °C. ^1H NMR (400 MHz, $\text{DMSO}-d_6$) δ : 10.63 (s, 1H), 9.06 (d, J = 5.6 Hz, 1H), 7.67 (d, J = 16.7 Hz, 1H), 7.61–7.55 (d, J = 12.4 Hz, 5H), 7.24 (t, J = 8.5 Hz, 2H), 6.50 (d, J = 16.7 Hz, 1H), 4.65 (s, 2H), 2.13 (s, 6H). ^{13}C NMR (101 MHz, $\text{DMSO}-d_6$) δ : 169.07, 164.72, 161.29, 159.89, 158.87 (d, $J_{\text{C-F}}$ = 242.4 Hz) 150.97, 150.26, 135.06, 132.33, 131.35, 128.93, 121.49 (d, $J_{\text{C-F}}$ = 7.9 Hz), 119.27, 115.97 (d, $J_{\text{C-F}}$ = 22.4 Hz), 111.15, 97.32, 57.57, 16.37. HRMS (ESI) calcd for $\text{C}_{23}\text{H}_{19}\text{FN}_4\text{O}_4\text{S}$: 466.11, found: 489.100 $[\text{M} + \text{Na}]^+$.

4.8.2. (E)-N-(4-chlorophenyl)-2-((4-(4-(2-cyanovinyl)-2,6-dimethylphenoxy)pyrimidin-2-yl)sulfonyl)acetamide (41)

Yield: 54%. mp: 152.5–154.8 °C. ^1H NMR (400 MHz, $\text{DMSO}-d_6$) δ : 10.59 (s, 1H), 8.98 (d, J = 5.7 Hz, 1H), 7.60 (d, J = 16.7 Hz, 1H), 7.53–7.47 (m, 5H), 7.39 (s, 1H), 7.37 (s, 1H), 6.43 (d, J = 16.7 Hz, 1H), 4.58 (s, 2H), 2.05 (s, 6H). ^{13}C NMR (101 MHz, $\text{DMSO}-d_6$) δ : 169.06, 164.68, 161.30, 160.14, 150.96, 150.26, 137.58, 132.33, 131.34, 129.29, 128.92, 128.17, 121.23, 119.26, 111.18, 97.32, 57.64, 16.37. HRMS (ESI) calcd for $\text{C}_{23}\text{H}_{19}\text{ClN}_4\text{O}_4\text{S}$: 482.08, found: 505.069 $[\text{M} + \text{Na}]^+$.

4.8.3. (E)-2-((4-(4-(2-cyanovinyl)-2,6-dimethylphenoxy)pyrimidin-2-yl)sulfonyl)-N-(4-fluorobenzyl)acetamide (42)

Yield: 77%. mp: 130.7–132.0 °C. ^1H NMR (400 MHz, $\text{DMSO}-d_6$) δ : 8.95 (d, J = 5.7 Hz, 1H), 8.81 (t, J = 5.5 Hz, 1H), 7.61 (d, J = 16.7 Hz, 1H), 7.51 (s, 2H), 7.47 (d, J = 5.7 Hz, 1H), 7.31–7.21 (m, 2H), 7.14 (t, J = 8.7 Hz, 2H), 6.44 (d, J = 16.7 Hz, 1H), 4.42 (s, 2H), 4.22 (d, J = 5.7 Hz, 2H), 2.07 (s, 6H). ^{13}C NMR (101 MHz, $\text{DMSO}-d_6$) δ : 169.05, 164.80, 161.76 (d, $J_{\text{C-F}}$ = 244.4 Hz), 161.26, 161.16, 151.00, 150.24, 135.04 (d, $J_{\text{C-F}}$ = 3.0 Hz), 132.32, 131.98, 131.42, 129.69 (d, $J_{\text{C-F}}$

$F = 8.1$ Hz), 129.14, 128.91, 119.26, 115.52 (d, $J_{C-F} = 21.3$ Hz), 111.02, 97.33, 56.63, 42.06, 16.37. LCMS (ESI) calcd for $C_{24}H_{21}FN_4O_4S$: 480.13, found: 503.609 [M + Na]⁺.

4.8.4. (E)-N-(4-chlorobenzyl)-2-((4-(2-cyanovinyl)-2,6-dimethylphenoxy)pyrimidin-2-yl)sulfonyl)acetamide (43)

Yield: 73%. mp: 148.7–151.5 °C. ¹H NMR (400 MHz, DMSO-*d*₆) δ: 8.95 (d, $J = 5.7$ Hz, 1H), 8.85 (t, $J = 5.8$ Hz, 1H), 7.61 (d, $J = 16.7$ Hz, 1H), 7.51 (s, 2H), 7.47 (d, $J = 5.7$ Hz, 1H), 7.37 (d, $J = 8.4$ Hz, 2H), 7.25 (d, $J = 8.4$ Hz, 2H), 6.44 (d, $J = 16.7$ Hz, 1H), 4.42 (s, 2H), 4.23 (d, $J = 5.8$ Hz, 2H), 2.06 (s, 6H). ¹³C NMR (101 MHz, DMSO-*d*₆) δ: 169.05, 164.77, 161.34, 161.17, 151.00, 150.24, 137.95, 132.32, 132.03, 131.42, 129.53, 128.91, 128.72, 119.26, 111.04, 97.35, 56.64, 42.08, 16.38. LCMS (ESI) calcd for $C_{24}H_{21}ClN_4O_4S$: 496.10, found: 497.555 [M + H]⁺.

4.8.5. (E)-N-(4-bromobenzyl)-2-((4-(2-cyanovinyl)-2,6-dimethylphenoxy)pyrimidin-2-yl)sulfonyl)acetamide (44)

Yield: 60%. mp: 159.0–161.2 °C. ¹H NMR (400 MHz, DMSO-*d*₆) δ: 8.97 (d, $J = 5.7$ Hz, 1H), 8.88 (t, $J = 5.7$ Hz, 1H), 7.64 (d, $J = 16.7$ Hz, 1H), 7.53 (d, $J = 6.7$ Hz, 2H), 7.49 (d, $J = 5.7$ Hz, 1H), 7.21 (d, $J = 8.2$ Hz, 1H), 6.47 (d, $J = 16.7$ Hz, 1H), 4.45 (s, 2H), 4.23 (d, $J = 5.8$ Hz, 2H), 2.08 (s, 6H). ¹³C NMR (101 MHz, DMSO-*d*₆) δ: 169.06, 164.79, 161.36, 161.20, 151.02, 150.27, 138.42, 132.35, 131.66, 131.44, 129.93, 128.94, 120.51, 119.29, 111.06, 97.40, 56.65, 42.16, 16.41. HRMS (ESI) calcd for $C_{24}H_{21}BrN_4O_4S$: 540.05, found: 563.036 [M + Na]⁺.

4.8.6. (E)-2-((4-(2-cyanovinyl)-2,6-dimethylphenoxy)pyrimidin-2-yl)sulfonyl)-N-(4-fluorophenethyl)acetamide (45)

Yield: 75%. mp: 174.3–176.5 °C. ¹H NMR (400 MHz, DMSO-*d*₆) δ: 8.95 (d, $J = 5.7$ Hz, 1H), 8.40 (d, $J = 5.1$ Hz, 1H), 7.60 (d, $J = 16.7$ Hz, 1H), 7.51 (s, 2H), 7.47 (d, $J = 5.7$ Hz, 1H), 7.22 (dd, $J = 8.3, 5.8$ Hz, 2H), 7.09 (t, $J = 8.9$ Hz, 2H), 6.43 (d, $J = 16.7$ Hz, 1H), 4.32 (s, 2H), 3.21 (dd, $J = 12.8, 6.7$ Hz, 2H), 2.65 (t, $J = 7.0$ Hz, 2H), 2.08 (s, 6H). ¹³C NMR (101 MHz, DMSO-*d*₆) δ: 169.02, 164.82, 161.37 (d, $J_{C-F} = 242.4$ Hz), 161.16, 151.01, 150.23, 135.65 (d, $J_{C-F} = 3.0$ Hz), 132.33, 131.42, 130.95 (d, $J_{C-F} = 7.9$ Hz), 128.90, 119.25, 115.45 (d, $J_{C-F} = 21.0$ Hz), 110.97, 97.32, 56.54, 40.95, 34.26, 16.39. HRMS (ESI) calcd for $C_{25}H_{23}FN_4O_4S$: 494.14, found: 517.132 [M + Na]⁺.

4.8.7. (E)-N-(4-chlorophenethyl)-2-((4-(2-cyanovinyl)-2,6-dimethylphenoxy)pyrimidin-2-yl)sulfonyl)acetamide (46)

Yield: 80%. mp: 177.1–179.6 °C. ¹H NMR (400 MHz, DMSO-*d*₆) δ: 8.95 (d, $J = 5.7$ Hz, 1H), 8.38 (t, $J = 5.5$ Hz, 1H), 7.60 (d, $J = 16.7$ Hz, 1H), 7.51 (s, 2H), 7.47 (d, $J = 5.7$ Hz, 1H), 7.32 (d, $J = 8.3$ Hz, 2H), 7.21 (d, $J = 8.3$ Hz, 2H), 6.42 (d, $J = 16.7$ Hz, 1H), 4.32 (s, 2H), 3.22 (dd, $J = 12.9, 6.8$ Hz, 2H), 2.65 (t, $J = 7.0$ Hz, 2H), 2.08 (s, 6H). ¹³C NMR (101 MHz, DMSO-*d*₆) δ: 169.01, 164.80, 161.18, 151.01, 150.22, 138.54, 132.33, 131.42, 131.33, 131.08, 128.90, 128.69, 119.24, 110.98, 97.32, 56.55, 40.70, 34.37, 16.39. LCMS (ESI) calcd for $C_{25}H_{23}ClN_4O_4S$: 510.11, found: 511.555 [M + H]⁺.

4.8.8. (E)-N-(4-bromophenethyl)-2-((4-(2-cyanovinyl)-2,6-dimethylphenoxy)pyrimidin-2-yl)sulfonyl)acetamide (47)

Yield: 81%. mp: 182.8–185.4 °C. ¹H NMR (400 MHz, DMSO-*d*₆) δ: 8.95 (d, $J = 5.7$ Hz, 1H), 8.39 (t, $J = 5.4$ Hz, 1H), 7.60 (d, $J = 16.7$ Hz, 1H), 7.51 (s, 2H), 7.46 (t, $J = 6.8$ Hz, 3H), 7.15 (d, $J = 8.3$ Hz, 2H), 6.42 (d, $J = 16.7$ Hz, 1H), 4.32 (s, 2H), 3.22 (dd, $J = 12.8, 6.7$ Hz, 2H), 2.64 (t, $J = 7.0$ Hz, 2H), 2.08 (s, 6H). ¹³C NMR (101 MHz, DMSO-*d*₆) δ: 169.01, 164.80, 161.18, 151.01, 150.22, 138.96, 132.33, 131.61, 131.49, 131.42, 128.90, 119.79, 119.25, 110.98, 97.33, 56.54, 40.64, 34.43, 16.40. HRMS (ESI) calcd for $C_{25}H_{23}BrN_4O_4S$: 554.06, found: 577.050 [M + Na]⁺.

4.8.9. 2-((4-((4'-cyano-3,5-dimethyl-[1,1'-biphenyl]-4-yl)oxy)pyrimidin-2-yl)sulfonyl)-N-(4-fluorophenyl)acetamide (48)

Yield: 63%. mp: 158.3–160.8 °C. ¹H NMR (400 MHz, DMSO-*d*₆) δ: 10.47 (s, 1H), 8.98 (d, $J = 5.7$ Hz, 1H), 7.95–7.85 (m, 4H), 7.56 (s, 2H), 7.53–7.42 (m, 3H), 7.14 (t, $J = 8.8$ Hz, 2H), 4.60 (s, 2H), 2.12 (s, 6H). ¹³C NMR (101 MHz, DMSO-*d*₆) δ: 169.29, 164.83, 161.21, 158.87 (d, $J_{C-F} = 242.4$ Hz), 159.90, 149.59, 144.22, 136.59, 135.04 (d, $J_{C-F} = 2.5$ Hz), 133.20, 131.32, 128.15, 127.97, 121.48 (d, $J_{C-F} = 7.9$ Hz), 119.33, 115.94 (d, $J_{C-F} = 22.3$ Hz), 111.05, 110.51, 57.60, 16.51. HRMS (ESI) calcd for $C_{27}H_{21}FN_4O_4S$: 516.13, found: 539.116 [M + Na]⁺.

4.8.10. N-(4-chlorophenyl)-2-((4-((4'-cyano-3,5-dimethyl-[1,1'-biphenyl]-4-yl)oxy)pyrimidin-2-yl)sulfonyl)acetamide (49)

Yield: 75%. mp: 170.0–172.6 °C. ¹H NMR (400 MHz, DMSO-*d*₆) δ: 10.55 (s, 1H), 9.02–8.94 (m, 1H), 7.95–7.79 (m, 4H), 7.56–7.42 (m, 5H), 7.35 (d, $J = 7.5$ Hz, 2H), 4.62 (s, 2H), 2.12 (s, 6H). ¹³C NMR (101 MHz, DMSO-*d*₆) δ: 169.30, 164.82, 161.21, 160.15, 149.59, 144.21, 137.57, 136.59, 133.18, 131.30, 129.24, 128.20, 128.13, 127.95, 121.20, 119.33, 111.08, 110.51, 57.66, 16.52. HRMS (ESI) calcd for $C_{27}H_{21}ClN_4O_4S$: 532.10, found: 555.086 [M + Na]⁺.

4.8.11. N-(4-bromophenyl)-2-((4-((4'-cyano-3,5-dimethyl-[1,1'-biphenyl]-4-yl)oxy)pyrimidin-2-yl)sulfonyl)acetamide (50)

Yield: 66%. mp: 153.6–155.4 °C. ¹H NMR (400 MHz, DMSO-*d*₆) δ: 10.54 (s, 1H), 8.98 (d, $J = 5.7$ Hz, 1H), 7.90 (q, $J = 8.3$ Hz, 4H), 7.56 (s, 2H), 7.52–7.41 (m, 5H), 4.60 (s, 2H), 2.12 (s, 6H). ¹³C NMR (101 MHz, DMSO-*d*₆) δ: 169.28, 164.78, 161.23, 160.17, 149.59, 144.23, 137.98, 136.58, 133.22, 132.18, 131.31, 128.15, 127.97, 121.57, 119.34, 116.24, 111.11, 110.50, 57.66, 16.53. LCMS (ESI) calcd for $C_{27}H_{21}BrN_4O_4S$: 576.05, found: 599.901 [M + H]⁺.

4.8.12. 2-((4-((4'-cyano-3,5-dimethyl-[1,1'-biphenyl]-4-yl)oxy)pyrimidin-2-yl)sulfonyl)-N-(4-cyanophenyl)acetamide (51)

Yield: 65%. mp: 138.5–141.2 °C. ¹H NMR (400 MHz, DMSO-*d*₆) δ: 10.82 (s, 1H), 8.99 (d, $J = 5.7$ Hz, 1H), 7.88 (dd, $J = 18.4, 8.3$ Hz, 4H), 7.75 (d, $J = 8.6$ Hz, 2H), 7.64 (d, $J = 8.6$ Hz, 2H), 7.52 (s, 2H), 7.48 (d, $J = 5.7$ Hz, 1H), 4.67 (s, 2H), 2.11 (s, 6H). ¹³C NMR (101 MHz, DMSO-*d*₆) δ: 169.30, 164.76, 161.26, 160.87, 149.57, 144.18, 142.69, 136.57, 133.82, 133.18, 131.26, 128.12, 127.93, 119.75, 119.33, 119.28, 111.17, 110.51, 106.44, 57.70, 16.50. LCMS (ESI) calcd for $C_{28}H_{21}N_5O_4S$: 523.13, found: 524.672 [M + H]⁺.

4.8.13. 2-((4-((4'-cyano-3,5-dimethyl-[1,1'-biphenyl]-4-yl)oxy)pyrimidin-2-yl)sulfonyl)-N-(4-fluorobenzyl)acetamide (52)

Yield: 71%. mp: 156.7–159.0 °C. ¹H NMR (400 MHz, DMSO-*d*₆) δ: 8.95 (d, $J = 5.6$ Hz, 1H), 8.81 (d, $J = 5.2$ Hz, 1H), 7.92 (s, 4H), 7.60 (s, 2H), 7.45 (d, $J = 5.5$ Hz, 1H), 7.31–7.20 (m, 2H), 7.12 (t, $J = 8.6$ Hz, 2H), 4.45 (s, 2H), 4.23 (d, $J = 5.2$ Hz, 2H), 2.13 (s, 6H). ¹³C NMR (101 MHz, DMSO-*d*₆) δ: 169.27, 164.90, 161.74 (d, $J_{C-F} = 265.1$ Hz), 161.30, 161.11, 149.63, 144.24, 136.59, 135.04 (d, $J_{C-F} = 2.8$ Hz), 133.26, 131.41, 129.70 (d, $J_{C-F} = 8.1$ Hz), 128.16, 127.99, 119.35, 115.50 (d, $J_{C-F} = 21.2$ Hz), 110.93, 110.52, 56.62, 42.07, 16.52. HRMS (ESI) calcd for $C_{28}H_{23}FN_4O_4S$: 530.14, found: 553.131 [M + Na]⁺.

4.8.14. N-(4-chlorobenzyl)-2-((4-((4'-cyano-3,5-dimethyl-[1,1'-biphenyl]-4-yl)oxy)pyrimidin-2-yl)sulfonyl)acetamide (53)

Yield: 79%. mp: 166.3–168.9 °C. ¹H NMR (400 MHz, DMSO-*d*₆) δ: 8.95 (d, $J = 5.7$ Hz, 1H), 8.83 (t, $J = 5.6$ Hz, 1H), 7.93 (s, 4H), 7.61 (s, 2H), 7.46 (d, $J = 5.7$ Hz, 1H), 7.35 (d, $J = 8.3$ Hz, 2H), 7.24 (d, $J = 8.3$ Hz, 2H), 4.45 (s, 2H), 4.23 (d, $J = 5.7$ Hz, 2H), 2.13 (s, 6H). ¹³C NMR (101 MHz, DMSO-*d*₆) δ: 169.25, 164.87, 161.36, 161.11, 149.62, 144.25, 137.95, 136.59, 133.28, 132.02, 131.40, 129.54, 128.70, 128.16, 128.00, 119.34, 110.95, 110.53, 56.64, 42.09, 16.53. LCMS (ESI) calcd for $C_{28}H_{23}ClN_4O_4S$: 546.11, found: 569.697 [M + Na]⁺.

4.8.15. *N*-(4-bromobenzyl)-2-((4-((4'-cyano-3,5-dimethyl-[1,1'-biphenyl]-4-yl)oxy)pyrimidin-2-yl)sulfonyl)acetamide (54)

Yield: 60%. mp: 169.4–171.0 °C. ¹H NMR (400 MHz, DMSO-*d*₆) δ: 8.95 (d, *J* = 5.7 Hz, 1H), 8.84 (t, *J* = 5.6 Hz, 1H), 7.94 (d, *J* = 8.4 Hz, 4H), 7.60 (s, 2H), 7.47 (dd, *J* = 11.5, 7.0 Hz, 3H), 7.18 (d, *J* = 8.2 Hz, 2H), 4.45 (s, 2H), 4.21 (d, *J* = 5.7 Hz, 2H), 2.13 (s, 3H). ¹³C NMR (101 MHz, DMSO-*d*₆) δ: 169.25, 164.86, 161.37, 161.11, 149.62, 144.24, 138.38, 136.59, 133.28, 131.61, 131.41, 129.91, 128.15, 128.00, 120.49, 119.35, 110.96, 110.53, 56.63, 42.16, 16.53. LCMS (ESI) calcd for C₂₈H₂₃BrN₄O₄S: 590.06, found: 613.772 [M + Na]⁺.

4.8.16. 2-((4-((4'-cyano-3,5-dimethyl-[1,1'-biphenyl]-4-yl)oxy)pyrimidin-2-yl)sulfonyl)-*N*-(4-cyanobenzyl)acetamide (55)

Yield: 76%. mp: 174.8–176.5 °C. ¹H NMR (400 MHz, DMSO-*d*₆) δ: 8.95 (d, *J* = 5.8 Hz, 2H), 7.91 (s, 4H), 7.77 (d, *J* = 8.0 Hz, 2H), 7.59 (s, 2H), 7.47–7.39 (m, 3H), 4.50 (s, 2H), 4.34 (d, *J* = 5.6 Hz, 2H), 2.12 (s, 6H). ¹³C NMR (101 MHz, DMSO-*d*₆) δ: 169.28, 164.84, 161.60, 161.11, 149.60, 144.81, 144.21, 136.60, 133.26, 132.70, 131.39, 128.38, 128.14, 127.97, 119.35, 119.28, 110.98, 110.53, 110.22, 56.69, 42.49, 16.52. LCMS (ESI) calcd for C₂₉H₂₃N₅O₄S: 537.15, found: 538.609 [M + H]⁺.

4.8.17. 2-((4-((4'-cyano-3,5-dimethyl-[1,1'-biphenyl]-4-yl)oxy)pyrimidin-2-yl)sulfonyl)-*N*-(4-fluorophenethyl)acetamide (56)

Yield: 74%. mp: 155.3–157.2 °C. ¹H NMR (400 MHz, DMSO-*d*₆) δ: 9.05 (d, *J* = 5.7, 1H), 8.48 (s, 1H), 8.05–7.96 (m, 4H), 7.70 (s, 2H), 7.55 (d, *J* = 5.7, 1H), 7.35–7.26 (m, 2H), 7.16 (t, *J* = 8.7, 2H), 4.45 (s, 2H), 3.31 (dd, *J* = 12.9, 6.7, 2H), 2.74 (t, *J* = 7.0, 2H), 2.24 (s, 6H). ¹³C NMR (101 MHz, DMSO-*d*₆) δ: 169.32, 165.00, 161.44 (d, *J*_{C-F} = 242.4 Hz), 161.28, 161.20, 149.73, 144.33, 136.67, 135.73 (d, *J*_{C-F} = 3.0 Hz), 133.34, 131.49, 131.03 (d, *J*_{C-F} = 7.9 Hz), 128.24, 128.07, 119.43, 115.52 (d, *J*_{C-F} = 21.0 Hz), 110.98, 110.60, 56.65, 41.04, 34.35, 16.63. LCMS (ESI) calcd for C₂₉H₂₅FN₄O₄S: 544.16, found: 567.805 [M + Na]⁺.

4.8.18. *N*-(4-chlorophenethyl)-2-((4-((4'-cyano-3,5-dimethyl-[1,1'-biphenyl]-4-yl)oxy)pyrimidin-2-yl)sulfonyl)acetamide (57)

Yield: 53%. mp: 162.9–164.7 °C. ¹H NMR (400 MHz, DMSO-*d*₆) δ: 8.95 (d, *J* = 5.7 Hz, 1H), 8.39 (d, *J* = 5.4 Hz, 1H), 7.96–7.86 (m, 4H), 7.60 (s, 2H), 7.46 (d, *J* = 5.7 Hz, 1H), 7.29 (d, *J* = 8.3 Hz, 2H), 7.20 (d, *J* = 8.4 Hz, 2H), 4.35 (s, 2H), 3.22 (dd, *J* = 12.7, 6.7 Hz, 2H), 2.65 (t, *J* = 6.9 Hz, 2H), 2.14 (s, 6H). ¹³C NMR (101 MHz, DMSO-*d*₆) δ: 169.22, 164.89, 161.22, 161.11, 149.64, 144.24, 138.54, 136.58, 133.25, 131.40, 131.31, 131.07, 128.66, 128.15, 127.98, 119.34, 110.91, 110.51, 56.55, 40.71, 34.37, 16.54. HRMS (ESI) calcd for C₂₉H₂₅ClN₄O₄S: 560.13, found: 583.117 [M + Na]⁺.

4.8.19. *N*-(4-bromophenethyl)-2-((4-((4'-cyano-3,5-dimethyl-[1,1'-biphenyl]-4-yl)oxy)pyrimidin-2-yl)sulfonyl)acetamide (58)

Yield: 61%. mp: 165.3–167.9 °C. ¹H NMR (400 MHz, DMSO-*d*₆) δ: 8.95 (d, *J* = 5.7 Hz, 1H), 8.38 (t, *J* = 5.4 Hz, 1H), 7.91 (q, *J* = 8.4 Hz, 4H), 7.61 (s, 2H), 7.47 (d, *J* = 5.7 Hz, 1H), 7.42 (d, *J* = 8.2 Hz, 2H), 7.14 (d, *J* = 8.2 Hz, 2H), 4.34 (s, 2H), 3.22 (dd, *J* = 12.8, 6.6 Hz, 2H), 2.63 (t, *J* = 6.9 Hz, 2H), 2.15 (s, 6H). ¹³C NMR (101 MHz, DMSO-*d*₆) δ: 169.21, 164.88, 161.21, 161.11, 149.65, 144.24, 138.96, 136.58, 133.26, 131.58, 131.49, 131.40, 128.15, 127.99, 119.77, 119.35, 110.92, 110.51, 56.56, 40.64, 34.42, 16.55. LCMS (ESI) calcd for C₂₉H₂₅BrN₄O₄S: 604.08, found: 627.832 [M + Na]⁺.

4.8.20. *N*-(4-chlorophenyl)-2-((4-((4'-cyano-3,5-dimethyl-[1,1'-biphenyl]-4-yl)oxy)pyrimidin-2-yl)sulfonyl)propanamide (59)

Yield: 55%. mp: 117.0–118.3 °C. ¹H NMR (400 MHz, DMSO-*d*₆) δ: 10.52 (s, 1H), 8.97 (d, *J* = 5.7 Hz, 1H), 7.88 (q, *J* = 8.4 Hz, 4H), 7.58–7.52 (m, 4H), 7.45 (d, *J* = 5.7 Hz, 1H), 7.36 (d, *J* = 8.8 Hz, 2H), 4.69 (d, *J* = 7.0 Hz, 1H), 2.12 (s, 6H), 1.48 (d, *J* = 6.9 Hz, 3H). ¹³C NMR (101 MHz, DMSO-*d*₆) δ: 169.37, 164.52, 163.43, 161.22, 149.65, 144.23, 137.65, 136.68, 133.22, 131.32, 129.20, 128.16, 127.95,

121.42, 119.32, 111.21, 110.52, 63.31, 16.51, 12.74. HRMS (ESI) calcd for C₂₈H₂₃ClN₄O₄S: 546.11, found: 569.101 [M + Na]⁺.

4.8.21. 2-((4-((4'-cyano-3,5-dimethyl-[1,1'-biphenyl]-4-yl)oxy)pyrimidin-2-yl)sulfonyl)-*N*-(4-cyanophenyl)propanamide (60)

Yield: 61%. mp: 105.8–107.2 °C. ¹H NMR (400 MHz, DMSO-*d*₆) δ: 10.44 (s, 1H), 8.97 (d, *J* = 5.7 Hz, 1H), 7.89 (q, *J* = 8.1 Hz, 4H), 7.62–7.49 (m, 4H), 7.45 (d, *J* = 5.6 Hz, 1H), 7.15 (t, *J* = 8.7 Hz, 2H), 4.68 (q, *J* = 6.4 Hz, 1H), 2.12 (s, 6H), 1.48 (d, *J* = 6.8 Hz, 3H). ¹³C NMR (101 MHz, DMSO-*d*₆) δ: 169.36, 164.59, 163.22, 161.22, 160.08, 157.68, 149.65, 144.24, 136.69, 135.10, 133.23, 131.33, 128.17, 127.96, 121.75, 121.67, 119.32, 115.99, 115.77, 111.16, 110.52, 63.23, 16.49, 12.75. HRMS (ESI) calcd for C₂₉H₂₃N₅O₄S: 537.15, found: 536.14 [M - H]⁻.

4.8.22. 2-((4-((4'-cyano-3,5-dimethyl-[1,1'-biphenyl]-4-yl)oxy)pyrimidin-2-yl)sulfonyl)-*N*-(4-fluorobenzyl)propanamide (61)

Yield: 60%. mp: 197.4–200.1 °C. ¹H NMR (400 MHz, DMSO-*d*₆) δ: 8.95 (d, *J* = 5.6 Hz, 1H), 8.83 (s, 1H), 7.90 (q, *J* = 8.1 Hz, 4H), 7.59 (s, 2H), 7.46 (d, *J* = 5.6 Hz, 1H), 7.33 (d, *J* = 8.1 Hz, 2H), 7.25 (d, *J* = 8.1 Hz, 2H), 4.55 (q, *J* = 6.7 Hz, 1H), 4.31 (dd, *J* = 15.3, 5.9 Hz, 1H), 4.19 (dd, *J* = 15.3, 5.0 Hz, 1H), 2.14 (s, 6H), 1.41 (d, *J* = 6.9 Hz, 3H). ¹³C NMR (101 MHz, DMSO-*d*₆) δ: 169.28, 164.73, 164.69, 161.75 (d, *J*_{C-F} = 243.4 Hz), 161.08, 149.71, 144.27, 136.66, 135.15 (d, *J*_{C-F} = 2.8 Hz), 133.25, 131.40, 129.61 (d, *J*_{C-F} = 8.1 Hz), 128.15, 127.97, 119.34, 115.44 (d, *J*_{C-F} = 21.2 Hz), 111.12, 110.52, 62.35, 42.23, 16.52, 12.59. LCMS (ESI) calcd for C₂₉H₂₅FN₄O₄S: 544.16, found: 567.742 [M + Na]⁺.

4.8.23. *N*-(4-chlorobenzyl)-2-((4-((4'-cyano-3,5-dimethyl-[1,1'-biphenyl]-4-yl)oxy)pyrimidin-2-yl)sulfonyl)propanamide (62)

Yield: 72%. mp: 160.6–162.5 °C. ¹H NMR (400 MHz, DMSO-*d*₆) δ: 8.94 (d, *J* = 5.7 Hz, 1H), 8.80 (t, *J* = 5.3 Hz, 1H), 7.91 (q, *J* = 8.2 Hz, 4H), 7.60 (s, 2H), 7.46 (d, *J* = 5.6 Hz, 1H), 7.31–7.21 (m, 2H), 7.11 (t, *J* = 8.7 Hz, 2H), 4.54 (q, *J* = 6.7 Hz, 1H), 4.31 (dd, *J* = 15.1, 5.9 Hz, 1H), 4.18 (dd, *J* = 15.1, 5.0 Hz, 1H), 2.14 (s, 6H), 1.40 (d, *J* = 6.9 Hz, 3H). ¹³C NMR (101 MHz, DMSO-*d*₆) δ: 169.28, 164.76, 164.71, 161.08, 149.71, 144.26, 138.05, 136.66, 133.25, 131.97, 131.39, 129.49, 128.65, 128.14, 127.96, 119.34, 111.14, 110.52, 62.35, 42.29, 16.53, 12.56. LCMS (ESI) calcd for C₂₉H₂₅ClN₄O₄S: 560.13, found: 583.570 [M + Na]⁺.

4.8.24. *N*-(4-bromobenzyl)-2-((4-((4'-cyano-3,5-dimethyl-[1,1'-biphenyl]-4-yl)oxy)pyrimidin-2-yl)sulfonyl)propanamide (63)

Yield: 64%. mp: 132.1–133.9 °C. ¹H NMR (400 MHz, DMSO-*d*₆) δ: 8.95 (d, *J* = 5.7 Hz, 1H), 8.82 (t, *J* = 5.6 Hz, 1H), 7.90 (q, *J* = 8.5 Hz, 4H), 7.59 (s, 2H), 7.52–7.41 (m, 3H), 7.19 (d, *J* = 8.3 Hz, 2H), 4.54 (q, *J* = 6.9 Hz, 1H), 4.29 (dd, *J* = 15.4, 6.1 Hz, 1H), 4.17 (dd, *J* = 15.4, 5.3 Hz, 1H), 2.14 (s, 6H), 1.41 (d, *J* = 7.0 Hz, 3H). ¹³C NMR (101 MHz, DMSO-*d*₆) δ: 169.28, 164.76, 164.70, 161.08, 149.71, 144.26, 138.49, 136.66, 133.26, 131.57, 131.40, 129.87, 128.15, 127.97, 120.42, 119.34, 111.14, 110.53, 62.35, 42.34, 16.54, 12.56. HRMS (ESI) calcd for C₂₉H₂₅BrN₄O₄S: 604.08, found: 627.067 [M + Na]⁺.

4.8.25. 2-((4-((4'-cyano-3,5-dimethyl-[1,1'-biphenyl]-4-yl)oxy)pyrimidin-2-yl)sulfonyl)-*N*-(1-(4-fluorophenyl)ethyl)acetamide (64)

Yield: 83%. mp: 101.8–103.5 °C. ¹H NMR (400 MHz, DMSO-*d*₆) δ: 8.93 (d, *J* = 5.7 Hz, 1H), 8.78 (d, *J* = 7.8 Hz, 1H), 7.98–7.88 (m, 4H), 7.60 (s, 2H), 7.43 (d, *J* = 5.7 Hz, 1H), 7.31 (dd, *J* = 8.5, 5.6 Hz, 2H), 7.13 (t, *J* = 8.9 Hz, 2H), 4.80 (t, *J* = 7.2 Hz, 1H), 4.42 (s, 2H), 2.11 (s, 6H), 1.32 (d, *J* = 7.0 Hz, 3H). ¹³C NMR (101 MHz, DMSO-*d*₆) δ: 169.23, 164.89, 161.56 (d, *J*_{C-F} = 246.4 Hz), 161.08, 149.61, 144.25, 140.19 (d, *J*_{C-F} = 3.0 Hz), 136.58, 133.28, 131.40, 128.36 (d, *J*_{C-F} = 8.1 Hz), 128.16, 128.00, 119.34, 115.43 (d, *J*_{C-F} = 21.2 Hz), 110.86, 110.53, 56.59, 48.19, 22.70, 16.51. LCMS (ESI) calcd for C₂₉H₂₅FN₄O₄S: 544.16, found: 567.742 [M + Na]⁺.

4.8.26. *N*-(1-(4-chlorophenyl)ethyl)-2-((4-((4'-cyano-3,5-dimethyl-[1,1'-biphenyl]-4-yl)oxy)pyrimidin-2-yl)sulfonyl)acetamide (**65**)

Yield: 76%. mp: 140.6–142.9 °C. ¹H NMR (400 MHz, DMSO-*d*₆) δ: 8.93 (d, *J* = 5.7 Hz, 1H), 8.81 (d, *J* = 7.7 Hz, 1H), 7.98–7.88 (m, 4H), 7.60 (s, 2H), 7.43 (d, *J* = 5.7 Hz, 1H), 7.36 (d, *J* = 8.5 Hz, 2H), 7.30 (d, *J* = 8.4 Hz, 2H), 4.88–4.71 (m, 1H), 4.42 (s, 2H), 2.11 (s, 6H), 1.32 (d, *J* = 7.0 Hz, 3H). ¹³C NMR (101 MHz, DMSO-*d*₆) δ: 169.23, 164.87, 161.08, 160.41, 149.60, 144.25, 143.08, 136.59, 133.28, 131.85, 131.40, 128.68, 128.30, 128.14, 128.00, 119.34, 110.87, 110.54, 56.59, 48.30, 22.55, 16.51. LCMS (ESI) calcd for C₂₉H₂₅ClN₄O₄S: 560.13, found: 583.633 [M + Na]⁺.

4.8.27. *N*-(1-(4-bromophenyl)ethyl)-2-((4-((4'-cyano-3,5-dimethyl-[1,1'-biphenyl]-4-yl)oxy)pyrimidin-2-yl)sulfonyl)acetamide (**66**)

Yield: 74%. mp: 137.5–139.0 °C. ¹H NMR (400 MHz, DMSO-*d*₆) δ: 8.93 (d, *J* = 5.7 Hz, 1H), 8.81 (d, *J* = 7.6 Hz, 1H), 7.98–7.89 (m, 4H), 7.60 (s, 2H), 7.50 (d, *J* = 8.3 Hz, 2H), 7.43 (d, *J* = 5.7 Hz, 1H), 7.24 (d, *J* = 8.4 Hz, 2H), 4.84–4.70 (m, 1H), 4.42 (s, 2H), 2.10 (s, 6H), 1.31 (d, *J* = 7.0 Hz, 3H). ¹³C NMR (101 MHz, DMSO-*d*₆) δ: 169.22, 164.87, 161.08, 160.42, 149.60, 144.24, 143.53, 136.59, 133.29, 131.60, 131.40, 128.68, 128.14, 128.01, 120.32, 119.34, 110.88, 110.54, 56.58, 48.37, 22.51, 16.51. HRMS (ESI) calcd for C₂₉H₂₅BrN₄O₄S: 604.08, found: 629.064 [M + Na]⁺.

4.9. Antiviral activity assays

4.9.1. *In vitro* anti-HIV assay

Evaluation of the antiviral activity of the compounds against wild-type HIV-1, and mutant strains (L100I, K103N, Y181C, Y188L, E138K, F227L + V106A, and RES056) in MT-4 cells was performed using the MTT assay as previously described [35]. Stock solutions (10 × final concentration) of test compounds were added in 25 μL volumes to two series of triplicate wells so as to allow simultaneous evaluation of their effects on mock- and HIV-infected cells at the beginning of each experiment. Serial 5-fold dilutions of test compounds were made directly in flat-bottomed 96-well microtiter trays using a Biomek 3000 robot (Beckman instruments, Fullerton, CA). Untreated HIV- and mock-infected cell samples were included as controls. HIV stock (50 μL) at 100–300 CCID₅₀ (50% cell culture infectious doses) or culture medium was added to either the infected or mock-infected wells of the microtiter tray. Mock-infected cells were used to evaluate the effects of test compound on uninfected cells in order to assess the cytotoxicity of the test compounds. Exponentially growing MT-4 cells were centrifuged for 5 min at 220 g and the supernatant was discarded. The MT-4 cells were resuspended at 6 × 10⁵ cells/ml and 50 μL volumes were transferred to the microtiter tray wells. Five days after infection, the viability of mock- and HIV-infected cells was examined spectrophotometrically using the MTT assay. The MTT assay is based on the reduction of yellow colored 3-(4,5-dimethylthiazol-2-yl)-2,5-diphenyltetrazolium bromide (MTT) (Acros Organics) by mitochondrial dehydrogenase activity in metabolically active cells to a blue-purple formazan that can be measured spectrophotometrically. The absorbances were read in an eight-channel computer-controlled photometer (Infinite M1000, Tecan), at two wavelengths (540 and 690 nm). All data were calculated using the median absorbance value of three wells. The 50% cytotoxic concentration (CC₅₀) was defined as the concentration of the test compound that reduced the absorbance (OD540) of the mock-infected control sample by 50%. The concentration achieving 50% protection against the cytopathic effect of the virus in infected cells was defined as the 50% effective concentration (EC₅₀).

4.9.2. HIV-1 RT inhibition assay

Recombinant wild type p66/p51 HIV-1 RT was expressed and purified as previously described [36]. The RT assay was performed with the EnzCheck Reverse Transcriptase Assay kit (Molecular Probes, Invitrogen), as described by the Manufacturer. The assay was based on

the dsDNA quantitation reagent PicoGreen. This reagent shows a pronounced increase in fluorescence signal upon binding to dsDNA or RNA-DNA heteroduplexes. Single-stranded nucleic acids generate only minor fluorescence signal enhancement when a sufficiently high dye:base pair ratio is applied [37]. This condition was met in the assay. A poly(rA) template of approximately 350 bases long, and an oligo(dT)16 primer, were annealed in a molar ratio of 1:1.2 (60 min. at room temperature). Fifty-two ng of the RNA/DNA was brought into each well of a 96-well plate in a volume of 20 μL polymerization buffer (60 mM Tris-HCl, 60 mM KCl, 8 mM MgCl₂, 13 mM DTT, 100 μM dTTP, pH 8.1). 5 μL of RT enzyme solution, diluted to a suitable concentration in enzyme dilution buffer (50 mM Tris-HCl, 20% glycerol, 2 mM DTT, pH 7.6), is added. The reaction mixtures were incubated at 25 °C for 40 min and then stopped by the addition of EDTA (15 mM final). Heteroduplexes were then detected by addition of PicoGreen. Signals were read using an excitation wavelength of 490 nm and emission detection at 523 nm using a spectrofluorometer (Safire 2, Tecan). To test the activity of compounds against RT, 1 μL of compound in DMSO was added to each well before the addition of RT enzyme solution. Control wells without compound contain the same amount of DMSO. Results are expressed as relative fluorescence i.e. the fluorescence signal of the reaction mix with compound divided by the signal of the same reaction mix without compound.

4.10. Molecular modeling

Molecular modelling research work was performed with the Tripos molecular modelling software package (Sybyl-X 2.0). All the molecules for docking analysis were built using the standard bond lengths and angles from Sybyl-X 2.0/base Builder before being optimized using the Tripos force field for 10,000 generations two times or more, until the minimized conformers of the ligand were the same. The flexible docking method, called Surflex-Dock, docks the ligand automatically into the ligand binding site of the receptor by using a protocol-based approach and an empirically-derived scoring function. The protocol is a computational representation of a putative ligand that binds to the intended binding site and is a unique and essential element of the docking algorithm. The scoring function in Surflex-Dock, which contained hydrophobic, polar, repulsive, entropic, and solvation terms, was trained to estimate the dissociation constant (K_d) expressed in -log(K_d)². The scoring function in Surflex-Dock, which contains hydrophobic, polar, repulsive, entropic and solvation terms, was trained to estimate the binding energy. Prior to docking, the protein was prepared by removing water molecules, the ligand ETR, and other unnecessary small molecules from the crystal structure of the HIV-1 RT complex. Simultaneously, hydrogen atoms were added to the protein. Surflex-Dock default settings were used for other parameters, such as the number of starting conformations per molecule (set to 0), the size to expand search grid (set to 8 Å), the maximum number of the rotatable bonds per molecule (set to 100), and the maximum number of poses per ligand (set to 20). During the docking procedure, all of the single bonds in amino acid residue side-chains inside the defined RT binding pocket were regarded as rotatable or flexible, and the ligand was allowed to rotate at all single bonds and move flexibly within the tentative binding pocket. The atomic charges were recalculated using the Kollman all-atom approach for the protein and the Gasteiger-Hückel approach for the ligand. The binding interaction energy was calculated, including van der Waals, electrostatic, and torsional energy terms defined in the Tripos force field. The structure optimization was performed for more than 10,000 generations using a genetic algorithm, and the 20-best-scoring ligand-protein complexes were kept for the further analyses. The -log(K_d)² values of the 20-best-scoring complexes, which represented the binding affinities of the ligand with RT, encompassed a wide scope of the functional classes (10⁻²-10⁻⁹). Only the highest scoring 3D structural model of the ligand-bound RT was chosen to define the binding interaction.

Declaration of Competing Interest

The authors declare that they have no known competing financial interests or personal relationships that could have appeared to influence the work reported in this paper.

Acknowledgments

We gratefully acknowledge the generous support provided by the National Natural Science Foundation of P. R. China (81872791, 21372050) and the Young Elite Scientists Sponsorship Program by the China Association for Science and Technology (2017QNRC061). The technical assistance of Mr. Kris Uyttersprot, Mrs. Kristien Erven, and Mrs. Cindy Heens for the HIV experiments and HIV RT polymerase assays is gratefully acknowledged.

Appendix A. Supplementary material

Supplementary data to this article can be found online at <https://doi.org/10.1016/j.bioorg.2020.103595>.

References

- [1] UNAIDS (last accessed January 8, 2020), <https://www.unaids.org/en/resources/documents/2019/2019-UNAIDS-data>.
- [2] S.K. Vernekar, Z. Liu, E. Nagy, L. Miller, K.A. Kirby, D.J. Wilson, J. Kankanala, S.G. Sarafianos, M.A. Parniak, Z. Wang, Design, synthesis, biochemical, and antiviral evaluations of C6 benzyl and C6 biaryl methyl substituted 2-hydroxyisoquinoline-1,3-diones: dual inhibition against HIV reverse transcriptase-associated RNase H and polymerase with antiviral activities, *J. Med. Chem.* 58 (2015) 651–664.
- [3] G.A. Freeman, C.W. Andrews 3rd, A.L. Hopkins, G.S. Lowell, L.T. Schaller, J.R. Cowan, S.S. Gonzales, G.W. Koszalka, R.J. Hazen, L.R. Boone, R.G. Ferris, K.L. Creech, G.B. Roberts, S.A. Short, K. Weaver, D.J. Reynolds, J. Milton, J. Ren, D.I. Stuart, D.K. Stammers, J.H. Chan, Design of non-nucleoside inhibitors of HIV-1 reverse transcriptase with improved drug resistance properties, *J. Med. Chem.* 47 (2004) 5923–5936.
- [4] D. Kang, H. Zhang, Z. Wang, T. Zhao, T. Ginex, F.J. Luque, Y. Yang, G. Wu, D. Feng, F. Wei, J. Zhang, E. De Clercq, C. Pannecouque, C.H. Chen, K.H. Lee, N.A. Murugan, T.A. Steitz, P. Zhan, X. Liu, Identification of Dihydrofuro[3,4-d]pyrimidine Derivatives as Novel HIV-1 non-nucleoside reverse transcriptase inhibitors with promising antiviral activities and desirable physicochemical properties, *J. Med. Chem.* 62 (2019) 1484–1501.
- [5] Z. Fang, Y. Song, P. Zhan, Q. Zhang, X. Liu, Conformational restriction: an effective tactic in 'follow-on'-based drug discovery, *Future Med. Chem.* 6 (2014) 885–901.
- [6] P. Zhan, X. Chen, D. Li, Z. Fang, E. De Clercq, X. Liu, HIV-1 NNRTIs: structural diversity, pharmacophore similarity, and implications for drug design, *Med. Res. Rev.* 33 (2013) E1–E72.
- [7] K.D. Asgaonkar, S.M. Patil, T.S. Chitre, V.N. Ghegade, S.R. Jadhav, S.S. Sande, A.S. Kulkarni, Comparative docking studies: a drug design tool for some pyrazine-thiazolidinone based derivatives for anti-HIV activity, *Curr. Comput. Aided Drug Des.* 15 (2019) 252–258.
- [8] G. Costa, R. Rocca, A. Corona, N. Grandi, F. Moraca, I. Romeo, C. Talarico, M.G. Gagliardi, F.A. Ambrosio, F. Ortuso, S. Alcaro, S. Distinto, E. Maccioni, E. Tramontano, A. Artese, Novel natural non-nucleoside inhibitors of HIV-1 reverse transcriptase identified by shape- and structure-based virtual screening techniques, *Eur. J. Med. Chem.* 161 (2019) 1–10.
- [9] B. Huang, W. Chen, T. Zhao, Z. Li, X. Jiang, T. Ginex, D. Vilchez, F.J. Luque, D. Kang, P. Gao, J. Zhang, Y. Tian, D. Daelemans, E. De Clercq, C. Pannecouque, P. Zhan, X. Liu, Exploiting the Tolerant Region I of the Non-Nucleoside Reverse Transcriptase Inhibitor (NNRTI) binding pocket: discovery of potent diarylpyrimidine-Typed HIV-1 NNRTIs against Wild-Type and E138K mutant virus with significantly improved water solubility and favorable safety profiles, *J. Med. Chem.* 62 (2019) 2083–2098.
- [10] M. Udier-Blagovic, J. Tirado-Rives, W.L. Jorgensen, Validation of a model for the complex of HIV-1 reverse transcriptase with nonnucleoside inhibitor TMC125, *J. Am. Chem. Soc.* 125 (2003) 6016–6017.
- [11] N.G. Sharaf, R. Ishima, A.M. Gronenborn, Conformational Plasticity of the NNRTI-Binding Pocket in HIV-1 reverse transcriptase: a fluorine nuclear magnetic resonance study, *Biochemistry* 55 (2016) 3864–3873.
- [12] K.A. Paris, O. Haq, A.K. Felts, K. Das, E. Arnold, R.M. Levy, Conformational landscape of the human immunodeficiency virus type 1 reverse transcriptase non-nucleoside inhibitor binding pocket: lessons for inhibitor design from a cluster analysis of many crystal structures, *J. Med. Chem.* 52 (2009) 6413–6420.
- [13] V. Namasiyayam, M. Vanangamudi, V.G. Kramer, S. Kurup, P. Zhan, X. Liu, J. Kongsted, S.N. Byrareddy, The Journey of HIV-1 Non-Nucleoside Reverse Transcriptase Inhibitors (NNRTIs) from Lab to Clinic, *J. Med. Chem.* 62 (2019) 4851–4883.
- [14] A.M. Wensing, V. Calvez, H.F. Gunthard, V.A. Johnson, R. Paredes, D. Pillay, R.W. Shafer, D.D. Richman, Update of the drug resistance mutations in HIV-1, *Top. Antivir. Med.* 24 (2017) (2017) 132–133.
- [15] M. Baba, H. Tanaka, E. De Clercq, R. Pauwels, J. Balzarini, D. Schols, H. Nakashima, C.F. Perno, R.T. Walker, T. Miyasaka, Highly specific inhibition of human immunodeficiency virus type 1 by a novel 6-substituted acyclouridine derivative, *Biochem. Biophys. Res. Commun.* 165 (1989) 1375–1381.
- [16] R. Pauwels, K. Andries, J. Desmyter, D. Schols, M.J. Kukla, H.J. Breslin, A. Raeymaeckers, J. Van Gelder, R. Woestenborghs, J. Heykants, et al., Potent and selective inhibition of HIV-1 replication in vitro by a novel series of TIBO derivatives, *Nature* 343 (1990) 470–474.
- [17] E. De Clercq, Fifty years in search of selective antiviral drugs, *J. Med. Chem.* 62 (2019) 7322–7339.
- [18] C. Zhuang, C. Pannecouque, E. De Clercq, F. Chen, Development of non-nucleoside reverse transcriptase inhibitors (NNRTIs): our past twenty years, *Acta Pharm. Sin. B* (2019), <https://doi.org/10.1016/j.apbsb.2019.11.010>.
- [19] N. Pribut, A.E. Basson, W.A.L. van Otterlo, D.C. Liotta, S.C. Pelly, Aryl Substituted Benzimidazolones as Potent HIV-1 Non-Nucleoside Reverse Transcriptase Inhibitors, *ACS Med. Chem. Lett.* 10 (2019) 196–202.
- [20] Y. Sang, S. Han, C. Pannecouque, E. De Clercq, C. Zhuang, F. Chen, Ligand-based design of nondimethylphenyl-diarylpyrimidines with improved metabolic stability, safety and oral pharmacokinetic profiles, *J. Med. Chem.* (2019), <https://doi.org/10.1021/acs.jmedchem.9b01446>.
- [21] S. Han, Y. Sang, Y. Wu, Y. Tao, C. Pannecouque, E. De Clercq, C. Zhuang, F.E. Chen, Molecular hybridization-inspired optimization of diarylbenzopyrimidines as HIV-1 nonnucleoside reverse transcriptase inhibitors with improved activity against K103N and E138K mutants and pharmacokinetic profiles, *ACS Infect. Dis.* (2019), <https://doi.org/10.1021/acscinfdis.9b00229>.
- [22] Y. Sang, S. Han, C. Pannecouque, E. De Clercq, C. Zhuang, F. Chen, Conformational restriction design of thiophene-biphenyl-DAPY HIV-1 non-nucleoside reverse transcriptase inhibitors, *Eur. J. Med. Chem.* 182 (2019) 111603.
- [23] S. Kawamura, Y. Unno, A. Asai, M. Arisawa, S. Shuto, Structurally novel highly potent proteasome inhibitors created by the structure-based hybridization of non-peptidic belactosin derivatives and peptide boronates, *J. Med. Chem.* 57 (2014) 2726–2735.
- [24] J. Orbe, J.A. Sanchez-Arias, O. Rabal, J.A. Rodriguez, A. Salicio, A. Ugarte, M. Belzunce, M. Xu, W. Wu, H. Tan, H. Ma, J.A. Paramo, J. Oyarzabal, Design, synthesis, and biological evaluation of novel matrix metalloproteinase inhibitors as potent antihemorrhagic agents: from hit identification to an optimized lead, *J. Med. Chem.* 58 (2015) 2465–2488.
- [25] J.I. Montgomery, M.F. Brown, U. Reilly, L.M. Price, J.A. Abramite, J. Arcari, R. Barham, Y. Che, J.M. Chen, S.W. Chung, E.M. Collantes, C. Desbonnet, M. Doroski, J. Doty, J.J. Engtrakul, T.M. Harris, M. Huband, J.D. Knafels, K.L. Leach, S. Liu, A. Marfat, L. McAllister, E. McElroy, C.A. Menard, M. Mitton-Fry, L. Mullins, M.C. Noe, J. O'Donnell, R. Oliver, J. Penzien, M. Plummer, V. Shanmugasundaram, C. Thoma, A.P. Tomaras, D.P. Uccello, A. Vaz, D.G. Wishka, Pyridone methylsulfone hydroxamate LpxC inhibitors for the treatment of serious gram-negative infections, *J. Med. Chem.* 55 (2012) 1662–1670.
- [26] M. Allegretti, R. Bertini, M.C. Cesta, C. Bizzarri, R. Di Bitondo, V. Di Cioccio, E. Galliera, V. Berdini, A. Topai, G. Zampella, V. Russo, N. Di Bello, G. Nano, L. Nicolini, M. Locati, P. Fantucci, S. Florio, F. Colotta, 2-Arylpropionic CXC chemokine receptor 1 (CXCR1) ligands as novel noncompetitive CXCL8 inhibitors, *J. Med. Chem.* 48 (2005) 4312–4331.
- [27] J. Eron Jr., P. Yeni, J. Gathe Jr., V. Estrada, E. DeJesus, S. Staszewski, P. Lackey, C. Katlama, B. Young, L. Yau, D. Sutherland-Phillips, P. Wannamaker, C. Vavro, L. Patel, J. Yeo, M. Shaefer, K.s. team, The KLEAN study of fosamaprevir-ritonavir versus lopinavir-ritonavir, each in combination with abacavir-lamivudine, for initial treatment of HIV infection over 48 weeks: a randomised non-inferiority trial, *Lancet* 368 (2006) 476–482.
- [28] A.K. Ghosh, J.N. Williams, R.Y. Ho, H.M. Simpson, S.I. Hattori, H. Hayashi, J. Agniswamy, Y.F. Wang, I.T. Weber, H. Mitsuya, Design and Synthesis of Potent HIV-1 Protease Inhibitors Containing Bicyclic Oxazolindione Scaffold as the P2 Ligands: Structure-Activity Studies and Biological and X-ray Structural Studies, *J. Med. Chem.* 61 (2018) 9722–9737.
- [29] Z. Wan, J. Yao, T. Mao, X. Wang, H. Wang, W. Chen, H. Yin, F. Chen, E. De Clercq, D. Daelemans, C. Pannecouque, Pyrimidine sulfonylacetylides with improved potency against key mutant viruses of HIV-1 by specific targeting of a highly conserved residue, *Eur. J. Med. Chem.* 102 (2015) 215–222.
- [30] S. Han, Y. Sang, Y. Wu, Y. Tao, C. Pannecouque, E. De Clercq, C. Zhuang, F.-E. Chen, Fragment hopping-based discovery of novel sulfinylacetamide-diarylpyrimidines (DAPYs) as HIV-1 nonnucleoside reverse transcriptase inhibitors, *Eur. J. Med. Chem.* (2019), <https://doi.org/10.1016/j.ejmech.2019.111874>.
- [31] S. Han, Y. Lei, C. Pannecouque, E. De Clercq, C. Zhuang, F. Chen, Fragment-based discovery of sulfur-containing diarylbenzopyrimidines as novel nonnucleoside reverse transcriptase inhibitors, *Chin. Chem. Lett.* (2019), <https://doi.org/10.1016/j.ccl.2019.11.020>.
- [32] K. Jin, H. Yin, E. De Clercq, C. Pannecouque, G. Meng, F. Chen, Discovery of bi-phenyl-substituted diarylpyrimidines as non-nucleoside reverse transcriptase inhibitors with high potency against wild-type and mutant HIV-1, *Eur. J. Med. Chem.* 145 (2018) 726–734.
- [33] Y. Sang, S. Han, S. Han, C. Pannecouque, E. De Clercq, C. Zhuang, F. Chen, Follow on-based optimization of the biphenyl-DAPYs as HIV-1 nonnucleoside reverse transcriptase inhibitors against the wild-type and mutant strains, *Bioorg. Chem.* 89 (2019) 102974.
- [34] S. Kamijo, K. Kamijo, T. Murafuji, Synthesis of Alkylated Pyrimidines via Photoinduced Coupling Using Benzophenone as a Mediator, *J. Org. Chem.* 82 (2017) 2664–2671.

- [35] C. Pannecouque, D. Daelemans, E. De Clercq, Tetrazolium-based colorimetric assay for the detection of HIV replication inhibitors: revisited 20 years later, *Nat. Protoc.* 3 (2008) 427–434.
- [36] J. Auwerx, T.W. North, B.D. Preston, G.J. Klarmann, E. De Clercq, J. Balzarini, Chimeric human immunodeficiency virus type 1 and feline immunodeficiency virus reverse transcriptases: role of the subunits in resistance/sensitivity to non-nucleoside reverse transcriptase inhibitors, *Mol. Pharmacol.* 61 (2002) 400–406.
- [37] V.L. Singer, L.J. Jones, S.T. Yue, R.P. Haugland, Characterization of PicoGreen reagent and development of a fluorescence-based solution assay for double-stranded DNA quantitation, *Anal. Biochem.* 249 (1997) 228–238.